REPORT DOCUMENTATION PAGE

Form Approved
OMB NO. 0704-0188

1. AGENCY USE ONLY *(Leave blank)*	2. REPORT DATE	3. REPORT TYPE AND DATES COVERED
	May 25, 1996	Final Report 8/01/94-3/31/96

4. TITLE AND SUBTITLE
A Proposal to Extend the Visit of Professor V. F. Nesterenko at the University of California, San Diego

5. FUNDING NUMBERS
N00014-94-1-1040

6. AUTHOR(S)
M. A. Meyers and V. F. Nesterenko

7. PERFORMING ORGANIZATION NAMES(S) AND ADDRESS(ES)
University of California, San Diego
9500 Gilman Drive
Department of Applied Mechanics and Engineering Sciences
La Jolla, California 92093-0411

8. PERFORMING ORGANIZATION REPORT NUMBER

9. SPONSORING / MONITORING AGENCY NAME(S) AND ADDRESS(ES)
Office of Naval Research
Dr. Judah Goldwasser or Dr. R. Miller
Ballston Tower One
800 North Quincy Street
Arlington, Virginia 22217-5660

10. SPONSORING / MONITORING AGENCY REPORT NUMBER

11. SUPPLEMENTARY NOTES
The views, opinions and/or findings contained in this report are those of the author(s) and should not be construed as an official Department of the Army position, policy or decision, unless so designated by other documentation.

12a. DISTRIBUTION / AVAILABILITY STATEMENT
Approved for public release; distribution unlimited.

12 b. DISTRIBUTION CODE

13. ABSTRACT *(Maximum 200 words)*

The visit of Professor V. F. Nesterenko was successfully concluded and the principal objectives were accomplished. A collaborative effort on shock and shear initiated chemical reactions was started and is being continued. The focus of the work was on the Nb-Si and Ti-Si systems. A new methodology for investigating chemical reactions under shear was developed. Preliminary contacts with scientists at China Lake were established and are leading to continued collaboration. Professor Nesterenko was offered and accepted a position of Associate Professor at UCSD and is currently on the faculty of the Department of Applied Mechanics and Engineering Sciences.

14. SUBJECT TERMS			15. NUMBER IF PAGES
			16. PRICE CODE
17. SECURITY CLASSIFICATION OR REPORT	18. SECURITY CLASSIFICATION OF THIS PAGE	19. SECURITY CLASSIFICATION OF ABSTRACT	20. LIMITATION OF ABSTRACT
UNCLASSIFIED	UNCLASSIFIED	UNCLASSIFIED	UL

DISCLAIMER NOTICE

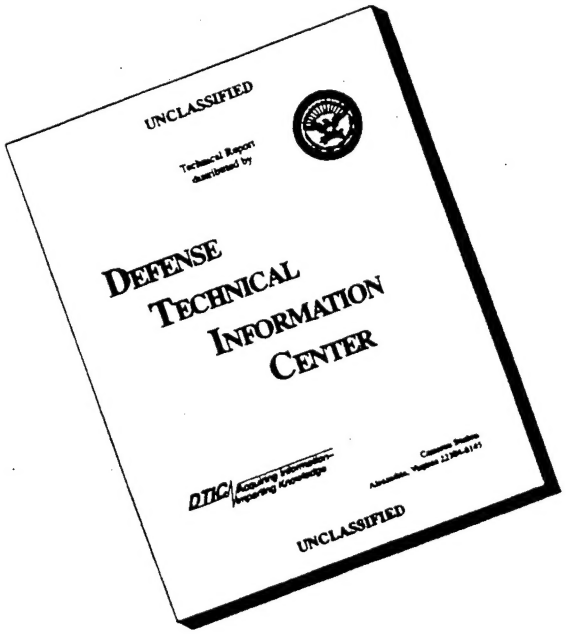

THIS DOCUMENT IS BEST QUALITY AVAILABLE. THE COPY FURNISHED TO DTIC CONTAINED A SIGNIFICANT NUMBER OF PAGES WHICH DO NOT REPRODUCE LEGIBLY.

TABLE OF CONTENTS

1. INTRODUCTION AND OBJECTIVES

It has been known for a long time that the collapse of voids (Bowden and Yoffe, 1958) and shear localization (Field, Swallowe, and Heavens, 1982) play a key role in the detonation of explosives. More recent results by Gilman (1995) indicate that shear strains produce the distortion of chemical bonds which directly affect the HOMO-LUMO gap in energetic materials, thereby accelerating the reaction rates. Experimental results on pore collapse in different materials by Nesterenko et al. (1993, 1994a,b) clearly demonstrate that shear localization phenomena accompany pore collapse as a result of material instability under high-strain-rate plastic flow. It has also been established that many exothermic reactions can be activated by the propagation of shock waves (Graham, 1993; Batsanov, 1993; Thadhani, 1994) and intense localized shear deformation (Nesterenko, Meyers, Chen, and LaSalvia, 1994, 1995, 1996; Chen, Meyers, and Nesterenko, 1995). In many underwater applications, it is desirable to control the chemical reaction rate(and, correspondingly the energy release rate) in order to optimize the efectiveness of the energetic material. The controlled high-strain -rate plastic deformation can be used additionally to shock wave loading for tailoring energy release in energetic materials.

II. BACKGROUND

Shock waves have been known to initiate chemical reactions in solids for a long time. The detonation of explosives is the classic example of this phenomenon. In more recent years, displacive phase transformations, decompositions, and chemical reactions have been induced by the propagation of shock waves. The first report of chemical changes occurring due to the application of shock compression is due to Russian scientist Ryabinin (1956). At the same time, Bancroft et al. (1957) described the alpha-epsilon phase transition undergone by iron at 13 GPa shock pressure. The synthesis of diamond from graphite, or directly from the detonation products of explosives, is a direct application of this concept. DeCarli and Jamieson (1961, 1966) in the early 1960s were the pioneers in this field having demonstrated that diamond particles (<10μm) could be produced from graphite. The early work by Nomura (1963, 1966) and Horiguchi (1966) in Japan, Adadurov et al. (1965) and Batsanov and Deribas (1965) and co-workers in Russia demonstrated that new compounds can be synthesized from powder mixtures through the propagation of a shock wave. A number of studies ensued, leading to the synthesis of numerous ceramic and intermetallic compounds via shock-induced chemical reactions between powders: silicides, aluminides, carbides, and other compounds. In the U.S., Graham (1986), Horie (1984, 1985, 1988) and co-workers played

a key role in shock synthesis. Lange and Ahrens (1986) studied the decomposition of $CaCO_3$ into CO_2 and CaO induced by shock waves; this study has important geological implications. Three books were recently published with strong emphasis on shock-induced reactions; Graham (1993), Horie and Sawaoka (1993), and Batsanov (1994). Additionally, the monograph by Thadhani (1992) is a comprehensive review. In 1984, the National Materials Advisory Board concluded a study on shock compression chemistry (Duvall, 1994).

Batsanov and co-workers (1986, 1991) reported anomalies in the pressure-volume Hugoniot curves produced by reactions. The pressure-volume curve for a reacting mixture shifted to the right, in analogy with explosives. This shift leads to alterations in pressure, particle velocity, and shock velocity, since a new thermodynamic state is accessed. Similar results were predicted by Boslough (1990) and Yu and Meyers (1991 developed) a simple thermodynamic treatment for the shock compression of reactive materials. They added the energy of reaction (E_r)to the conservation-of-energy equation:

$$E - E_0 = 1/2\ (P + P_0)(V_{00} - V) + E_r \qquad (1)$$

The Rankine-Hugoniot curves for solid, porous (powder) and reacted porous mixtures in the P-V plane are shown in Figure 1.

The P-V curve for the reactive mixture is translated to the right. If no reaction occurs, the shock pressure is given by P_1. The additional reaction energy, E_k, released increases the pressure in the powder to P'_1. If one draws a Rayleigh line through P'_1, one obtains a pressure P_2 after reaction (both shock and reaction front move at the same velocity in steady-state). One concludes that shock synthesis leads to an acceleration of reaction velocity with an increase in pressure. With the equation of state for the porous reacting material one can compute shock propagation velocities by means of Rayleigh lines. Fig. 1 also shows that P_t is required to induce reaction; if $P < P_t$, no reaction would occur.

Shock-induced reactions can be classified into two groups:

1. Synthesis: $x\,A + y\,B \rightarrow A_xB_y$.
2. Decomposition: $A_xB_y \rightarrow x\,A + y\,B$

where A and B can be elements or compounds.

Many exothermic reactions can be triggered by shock waves; a few examples are

$Ti + C \rightarrow TiC$ $\qquad$ $Ti + 2B \rightarrow TiB_2$

$xNi + yAl \rightarrow Ni_xAl_y$ $\qquad$ $xNb + yAl \rightarrow Nb_xAl_y$

$xNb + ySi \rightarrow Nb_xSi_y$ $\qquad$ $xTi + y\,\mathrm{Si} \rightarrow Ti_x\mathrm{Si}_y$

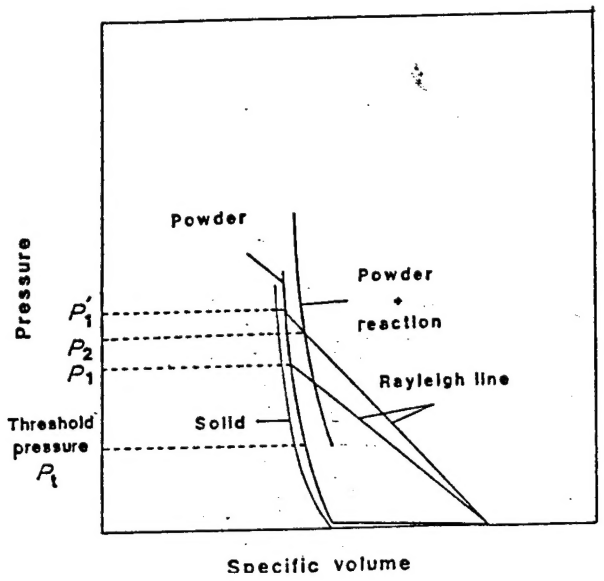

FIGURE 1. Schematic Hugoniots for solid, powder, and reacting powder (From L.H. Yu and M.A.Meyers, 1991).

A very important question is whether these reactions are only initiated by the shock wave or whether they proceed to their conclusion. After the passage of the shock wave the material is in a heated state due to shock and reaction heating, and this could lead to the continuation of the reaction.

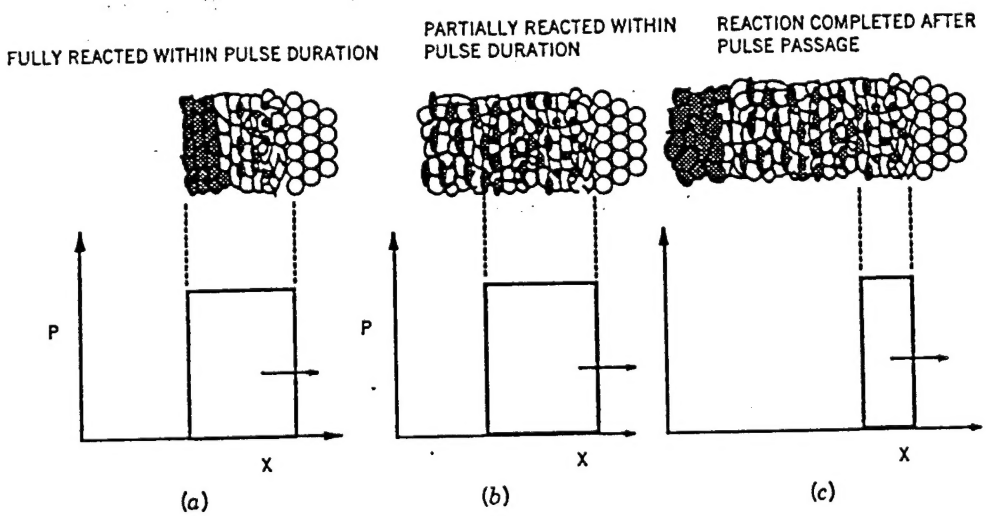

FIGURE 2. Propagation of shock wave through a reactive powder mixture with three possible situations schematically shown, dark regions represent reacted material: (a) material fully reacted within duration of pulse; (b) material partially reacted; (c) material fully reacted, with reaction initiated during shock pulse and terminating after this. (From M.A. Meyers, 1994).

Figure 2 shows, in a schematic fashion, the propagation of a shock wave through a porous reactive medium. The dark region represents reacted products. They increase in size with time. Three possible situations are depicted:

1. Materials is fully reacted within the duration of the pulse.
2. Material is partially reacted during duration of the pulse; reaction is stopped by release of pressure.
3. Material is partially reacted during duration of the pulse; reaction continues after pulse passage.

Thadhani (1993) classified these reactions into shock-induced (fully reacted during duration of pulse) and shock-assisted (reaction initiated by shock pulse). There are essentially two schools of thought regarding the onset of shock-induced chemical reactions: solid-solid vs. solid-liquid reactions. Graham (1993) and Batsanov (1994) provide substantial evidence in favor of the former mechanism whereas Krueger et al. (1991a,b, 1992), Vecchio et al. (1994), and Meyers et al. (1994) obtained results that substantiate a solid-liquid reaction.

At the microstructural level, these reactions are very complex and depend on a number of factors such as the porosity of material, size and shape of particles, shock pressure, and initial temperature. Meyers et al. (1994) and Vecchio et al. (1994) have addressed some of these issues in the development of a mechanism. Figure 3 shows a Mo + Si mixture. The photomicrograph shows unreacted (right) and partially reacted regions (left). The initial mixture was porous with separate Mo and Si powders. The reaction produces small spherical $MoSi_2$ particles; these particles are formed at the Mo-Si interface and "float" away, into silicon. It is thought that silicon melts and that a reaction between solid Nb and molten Si takes place under shock compression. These observations on Mo-Si and Nb-Si systems have been confirmed in other metal-silicon systems, indicating a common mechanism. Figures 4 and 5 show partially reacted regions for Ti-Si and W-Si systems at two different magnifications.

The Ti-Si reaction is highly exothermic (E_r = 580 kJ/mole) whereas the W-Si reaction is similar to the Nb-Si and Mo-Si reactions (E_r for Nb - Si is equal 138 kJ/mole). In the Ti-Si photomicrographs small elongated features (marked by arrows) are shown. They are clearly suggestive of melting. Meyers et al. (1994) developed an analytical framework based on these observations It is shown in Figure 6. This model assumes that silicon melts under the effect of shock compression, surrounding the solid Nb (or other metal) particles (Figure 6 (a)). The reaction product is liquid, due to the heat of reaction, increasing the temperature from the melting point of Si to the melting point of the reaction product. Surface (interface) tension

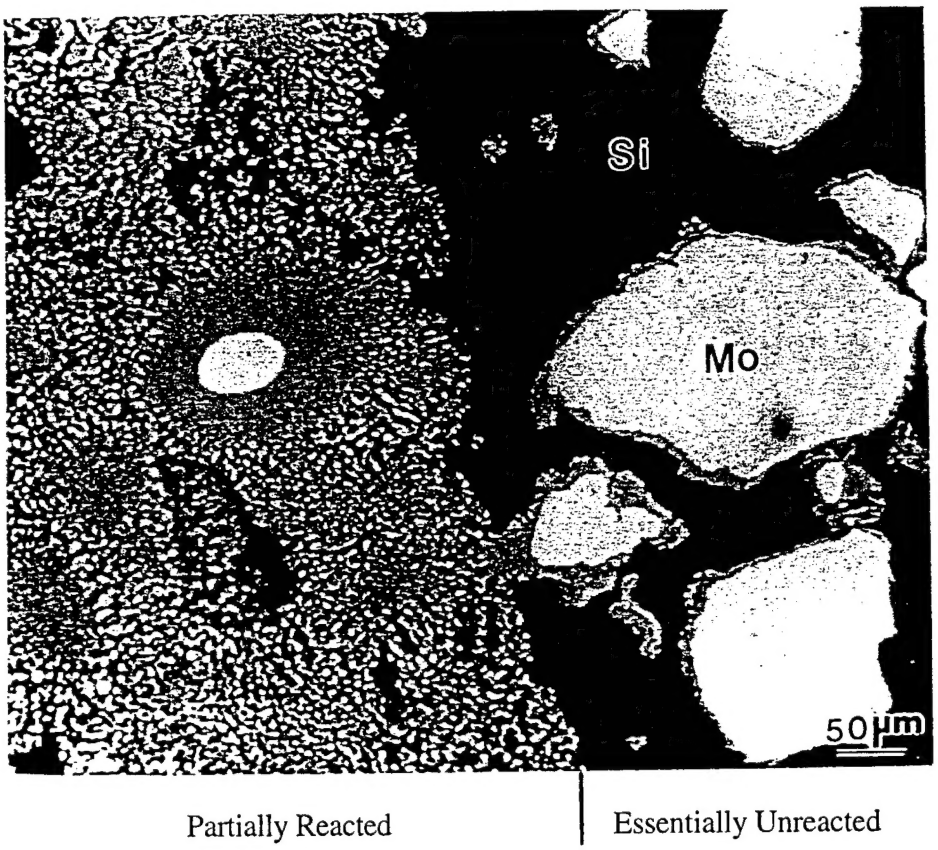

FIGURE 3. Interface between essentially unreacted and partially reacted areas in powder mixture Mo + 2Si.

forces act on the reaction product, turning it into spherules. This minimizes the interfacial energy. The spherules solidify (Fig. 6 (e)) and new spherules are formed, pushing the first generation ones away from interface. In this manner a continuous fresh reaction interface is maintained and the diffusion barrier from the reaction products is removed from interface. Thus, a high reaction rate can be maintained.

The seminal paper by Dremin and Breusov (1968) addresses the issue of shear deformation in shock processing to a considerable detail. The early work by Bridgman (1935, 1937, 1947, 1948) showed that shear deformation, superimposed on hydrostatic pressure, resulted in chemical reactions. Vereshchagin and co-workers (1960) confirmed the enhanced reactivity produced by shear deformation, and Teller (1962) supported the contention that reaction rates could be accelerated by shear deformation superimposed on high pressures. Enikolopyan and co-workers (1987, 1988, 1989) used a Bridgman cell and subjected a large number of chemical substances and mixtures to pressures, and simultaneous

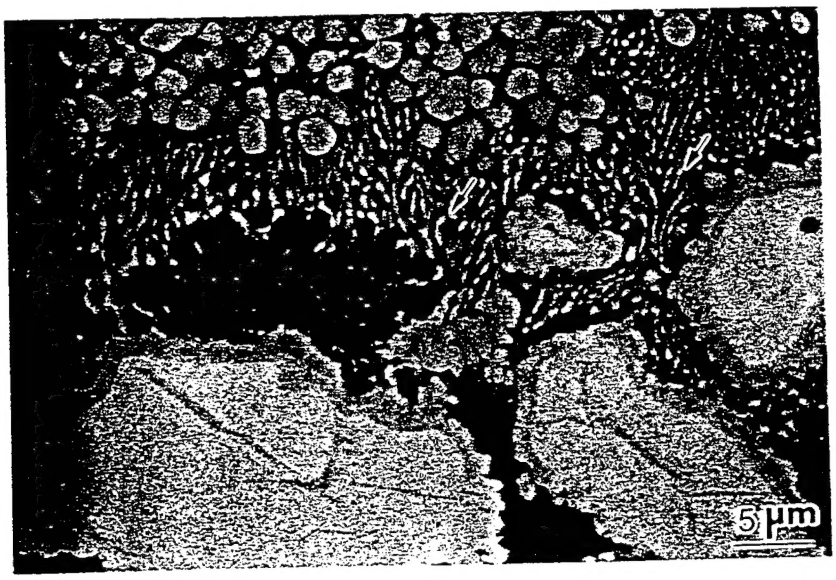

a

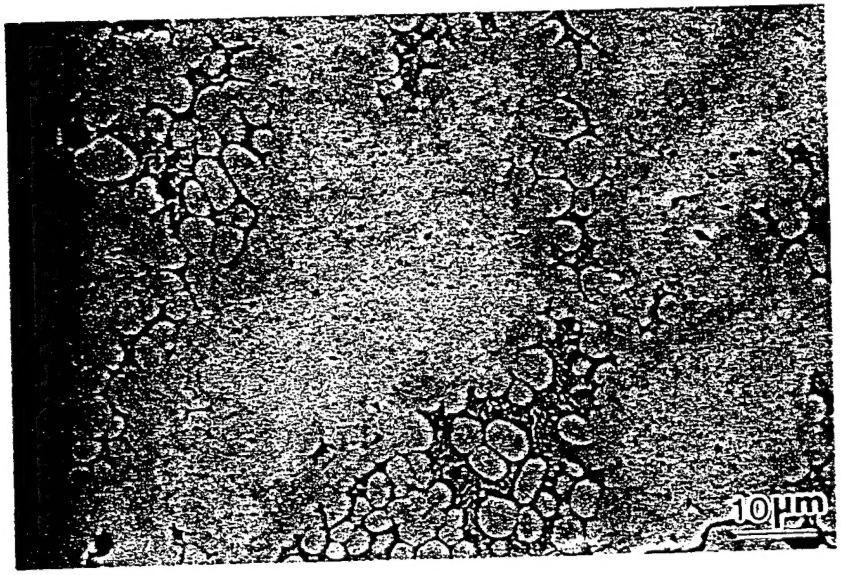

b

FIGURE 4. Partially reacted Ti + Si.

pressure and shear deformation. Their extensive studies confirmed the earlier findings of explosive reactions by Bridgman.

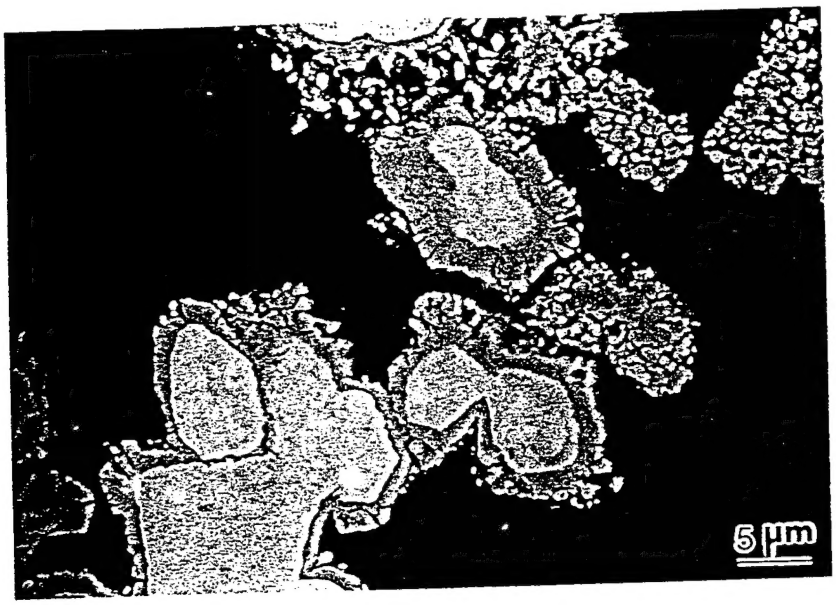

a

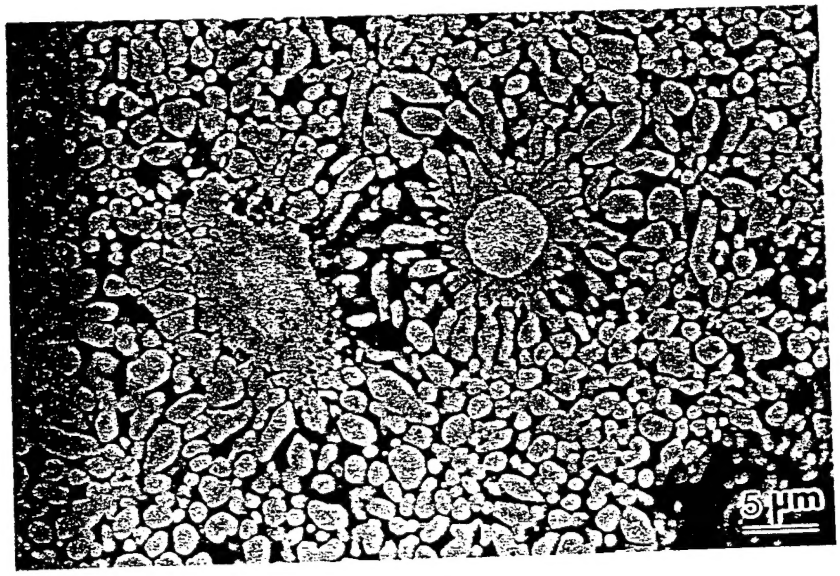

b

FIGURE 5. Partially reacted W + 2Si.

It was serendipitously discovered that plastic deformation, in addition to that normally occurring in the shock compression of powders, can have a significant effect on shock-induced chemical reactions. Shock densification experiments conducted on powder mixtures containing Mo and Si, or Nb and Si, revealed the formation of localized reaction regions in

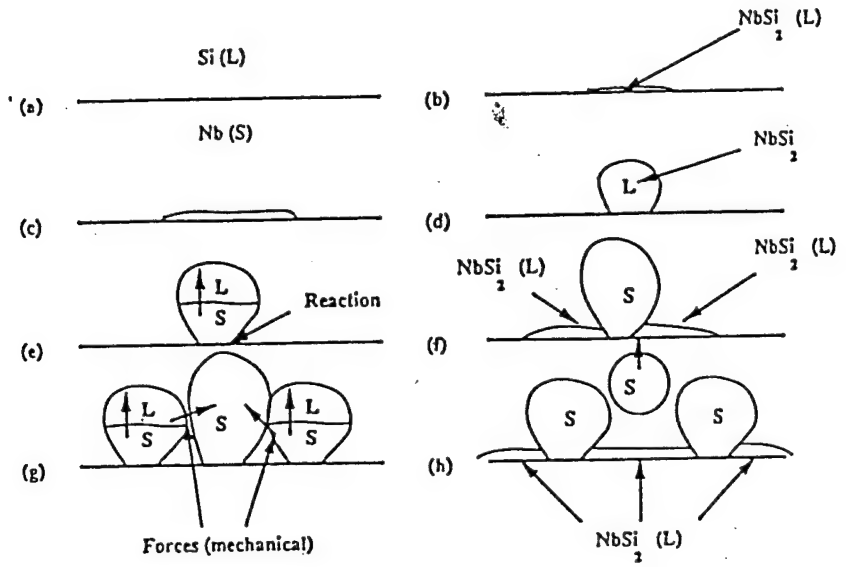

FIGURE 6. Sequence of events proposed by Meyers, Yu, and Vecchio (1994) for the formation of $NbSi_2$ spherules from the reaction of Nb and Si powders under shock compression. (a - c) nucleation and growth of thin layer; (d) interfacial energy producing spheroidization; (e) solidification of spherule due to reaction deceleration; (f - h) formation of spherules and their ejection from interface due to dissolution and mechanical forces.

narrow bands produced by shear localization (Meyers, 1994). Experiments also showed that plastic deformation influenced the reaction between elemental Nb and Si powders (Yu et al., 1994). Under shock pressure conditions which would not ordinarily result in reaction, localized regions in which the powder mixture had been intensely deformed plastically underwent chemical reaction. The powder mixture was extruded into the threaded regions by pressure differentials in capsule. The powder being deformed in the threaded regions reacted, because of the high local plastic strains. Nesterenko et al. (1994c) carried out controlled shear experiments, in the absence of shock compression, and demonstrated that reaction could take place.

The self-organization of shear-localization regions was established (Nesterenko, et al., 1994c, 1995, 1996) and the characteristic distance between shear bands was measured. The mechanism of reaction in the shear localization region is quite different from the one operating under shock loading conditions due to the relatively large displacements of neighboring particles, multiple fracturing and instability of shear flow.

III. EXPERIMENTAL APPROACH

In order to investigate the initiation of reaction in energetic materials we used the thick-walled cylinder method, initially developed for solid materials (Nesterenko, et al., 1989, 1993) and later modified (Nesterenko, Meyers et al., 1994, 1995) to accommodate porous mixtures. The main advantages of this method are:

- It ensures inertially confined high-strain-rate plastic flow of reactant material which can be represented as function of inner velocity of collapsing cylinder and can be changed by the variation of velocity and density of the driving cylinder;
- The global final plastic strain of reactant mixture and localized plastic deformation inside individual shear bands are measurable quantities;
- It is possible to precisely tune global plastic deformation, enabling the investigation of the threshold phenomena in reactant mixtures in a very narrow deformation window;
- The shock pressures in this method can be relatively small reproducing a real situation in applications;
- It is possible to combine the high-strain-rate plastic flow of reactant material with subsequent or preceding shock loading;
- The relative displacements inside shear bands are orders of magnitude higher than in shock-wave loading resulting in effective reaction initiation.

Three experimental configurations were used to generate controlled and prescribed shear localization in porous samples. They are shown in Figure 7. Details of the experimental set-up are presented in Figure 8.

In Configuration 1 (Figure 7a,b) a porous mixture is placed in a tubular cavity between a central copper rod and an outer copper tube. An explosive (explosive 1, Figure 7a) with a low detonation velocity (2.5 km/sec) is used to densify this mixture to a density ~75% of theoretical value. Detonation is initiated at the top of the charge and propagates along the cylinder axis. No shear localization is observed after this step because the global plastic deformation is sufficiently small . This stage only produces the densification of the powder mixture. A cylindrical hole is drilled along the longitudinal axis of copper rod and this composite cylinder is collapsed by the detonation of a second explosive charge (explosive 2, Fig. 7b) with a detonation velocity of 4 km/sec, an initial density of 1 g/cm^3, and an outer diameter of 60 mm (see Fig.8). This second explosive event produces significant plastic deformation in the densified porous layer which was highly localized in shear bands and not homogeneously distributed (Figure 9).

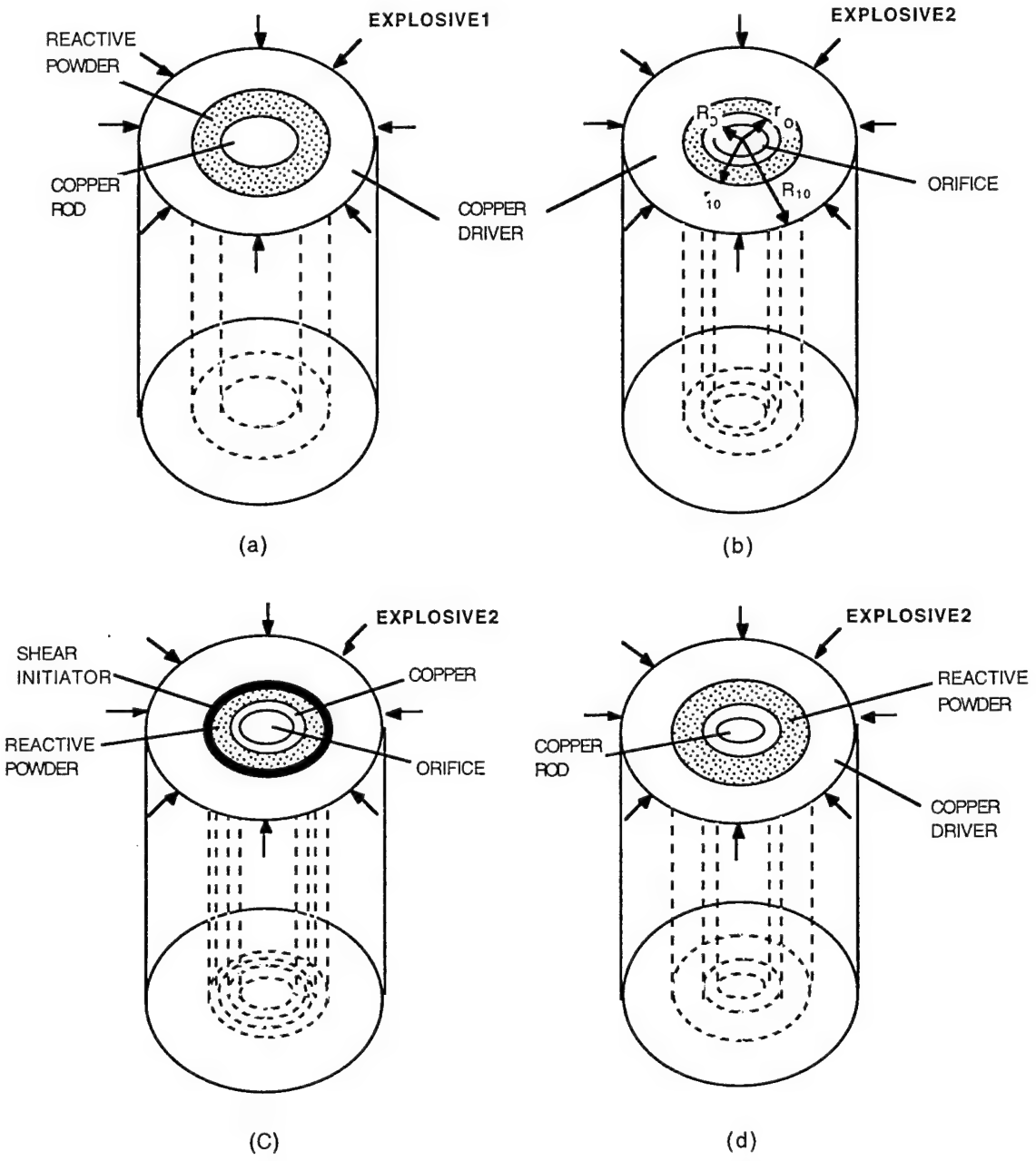

FIGURE 7. Geometry and sequence of deformation events in thick-walled cylinder method. Configuration 1: (a) initial geometry - densification by explosive 1: and (b) powder densified - after drilling of central orifice, cylinder collapsed by explosive 2. Configuration 2: (c) cylinder with orifice collapsed by explosive 2 with shear localization assistance by amorphous layer (shown by arrows). Configuration 3; (d) central rod tunes the global deformation of mixture.

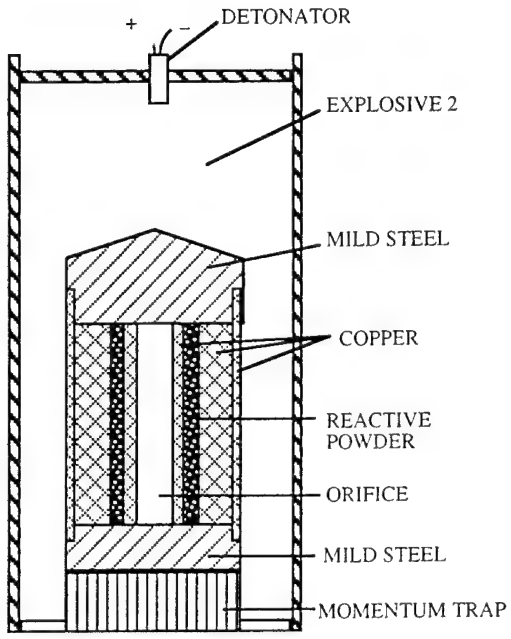

FIGURE 8. Overall experimental sketch for Configuration 1 (final phase) and Conf. 2.

Configuration 2 (Figure 7c) is used for the same powder as Configuration 1. The powder is placed in the tubular cavity. A preexisting hole along the longitudinal axis of assembly ensures high plastic deformation directly applied to the porous material. A few layers of amorphous ribbon (23 mm thick) can be placed along the cylinder walls to initiateshear localization in powder, with a lower density, at an early stage of collapse of inner hole. It has been established (Nesterenko and Pershin, 1989) that metallic glass foils undergo shear localization when dynamically deformed in a cylindrical geometry.

It is necessary to mention that the explosive parameters in the thick-walled cylinder method (detonation velocity, density, and thickness) should be carefully selected to provide a "smooth" pore collapse, by eliminating wave propagation effects, and by avoiding fracturing due to the spallation process and the radial cracks which can result from the back movement from the center after collapse. It is also necessary to minimize the effects of jet formation and the trapping of hot air in the center of the collapsing cylinder. The velocity of the inner wall during the collapse process was measured by the electromagnetic gage method (Nesterenko et al., 1993), providing information about overall strain and strain rate in reactant mixture.

Configuration 3 (Figure 7d) enables the control of the overall plastic deformation of material by selection of the appropriate inner rod diameter.

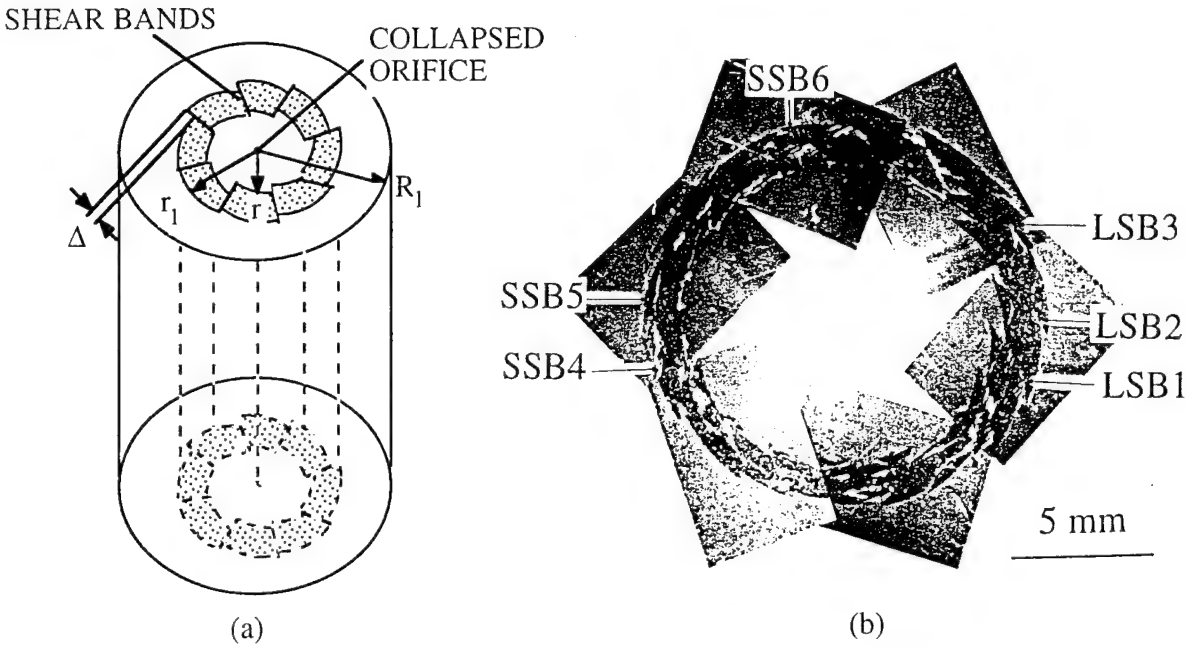

FIGURE 9. (a) - Schematic view of shear localization after cylinder collapse and (b) - overall view of shear localization after cylinder collapse in Configuration 1.

The global radial and tangential engineering strains (e_{rr} and $e_{\varphi\varphi}$) for an incompressible material, before the onset of localization, can be estimated knowing the initial and final radii, ρ_0 and ρ, at a general point:

$$e_{rr} = \frac{\rho_0}{\rho} - 1, \quad e_{\varphi\varphi} = \frac{\rho}{\rho_0} - 1 . \tag{2}$$

The global strains in the surfaces of copper cylinders restricting the porous tubular layer can be found from Eqns. 2. The final radii r and R (or R_1) and initial radius R_0 (or R_{10}) (Figure 7b) are experimentally measured and the value of ρ_0, which corresponds to a preselected value of ρ, can be calculated using Eqn.2:

$$\rho_0^2 = \rho^2 + R_0^2 - R^2 = \rho^2 + R_{10}^2 - R_1^2 , \tag{3}$$

where R and R_1 are final radii of inner hole and outer cylinder surface.

The strain state in cylindrical geometry in the uniformly deformed incompressible material is of pure shear and the deformation of an element is depicted in Figure 10. This type

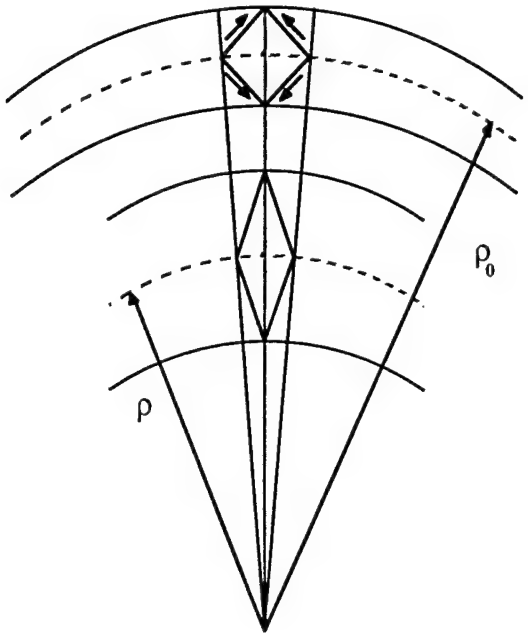

FIGURE 10. Geometry of pure shear in incompressible thick-walled cylindr under uniform plastic deformation; ρ_0 and ρ are the initial and final radii of one element, respectively.

of shear can be obtained by two systems of mutually perpendicular sets of slip planes, in comparison with one system for "simple shear". No rotation is associated with pure shear. In the experiments reported herein usually only one system of slip planes in given point of porous mixture was observed. Thus, locally the state of strain can be of simple shear after shear localization inside shear band.

The kinematics of uniform overall deformation can be determined from the measurement of the inner surface velocity of the wall, V_i . The radial and tangential strain rates (Figure 11) for the homogeneous collapse of the cylinder are :

$$\dot{e}_{rr} = -\frac{\left(\rho^2 + R_0^2\right)^{\frac{1}{2}}}{\left(\rho^2 + R^2(t)\right)^{\frac{3}{2}}} V_i(t)R(t),\ \dot{e}_{\varphi\varphi} = \frac{V_i(t)R(t)}{\left(\rho^2 + R_0^2\right)^{\frac{1}{2}}\left(\rho^2 + R^2(t)\right)^{\frac{1}{2}}} \qquad (4)$$

where $V_i(t)$ and $R(t)$ are the time-dependent velocities of inner surface and radius of hole, respectively. It is assumed that the hole is fully closed in the collapse process (i.e., R = 0)

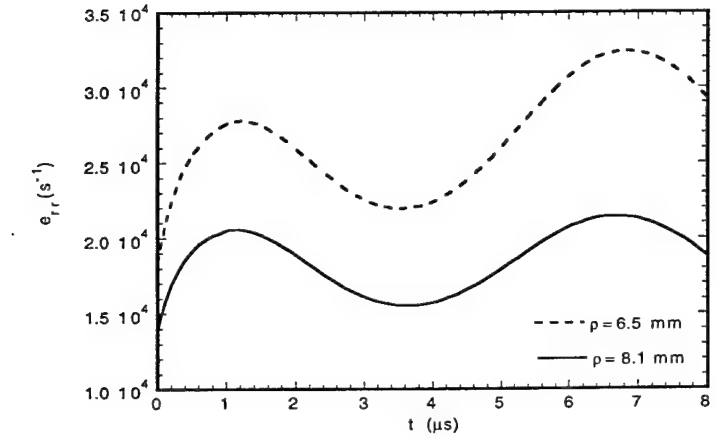

(a)

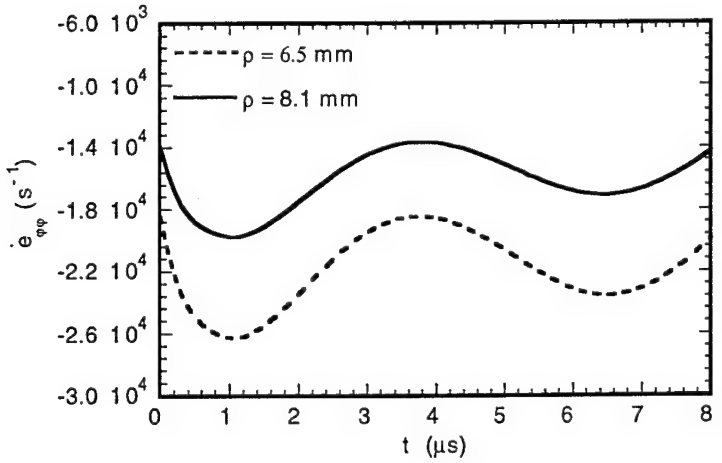

(b)

FIGURE 11. Global engineering strain rates for inner and outer surfaces of reactive porous cylindrical layer for Configuration 2.

and that it is not significantly altered by the insertion of the porous material layer; therefore measurements for copper cylinder were used. Strain rates, calculated from Eqns. 4, on the basis of the measurements of $V_i(t)$, are represented in Figure 11 for Configuration 2 for the inner and outer surfaces of the porous layer, corresponding to the uniform plastic

deformation. It is important to note that the overall strain rates in these points are relatively close and are in the range $(1.5\text{-}4)10^4\ s^{-1}$, as in Configuration 1.

From the measurements of the inner surface velocity, it is possible to calculate the inertial compression stress at the boundaries of the porous layer, representing inertial confinement. The pressure distribution in a collapsing incompressible ideal liquid cylinder with zero pressure on its surfaces is expressed by

$$p(\rho,R)=\frac{1}{2}d\,V_i^2\left[\left(1-\frac{R^2}{\rho^2}\right)-\left(1-\frac{R^2}{R_1^2}\right)\frac{\ln(\rho/R)}{\ln(R_1/R)}\right]$$

$$\left(\frac{\rho_m}{R}\right)^2=\left(1+\frac{R^2}{R_{10}^2-R_0^2}\right)\ln\left(1+\frac{R_{10}^2-R_0^2}{R^2}\right), \qquad (5)$$

where d is the density, r is the radius of one point inside the cylinder, V_i is the current velocity of inner surface, r_m is the radius corresponding to pressure maximum when radius of internal hole is equal to R (initial R_0) and outer radius is R_1 (initial R_{10}). For the conditions of Configurations 1 and 2 (initial velocity of inner surface 200 m/s), inertial compression stresses, calculated according to Eqns. 5, are found to be less than 0.1 GPa. This inertial confinement pressure can be changed by changing velocity of collapsing cylinder V_i and its density d.

Shear bands represent another scale of deformation events. The overall shear strain inside the shear zone(simple shear) is the ratio of the amplitude of shear, Δ (Figure 12) and thickness of shear band, δ:

$$\gamma \approx \frac{\Delta}{\delta} \qquad (6)$$

It is important to note that Configurations 1 and 2 yields "uniform" shear localization with approximately equal displacements ($\Delta \approx \Delta'$) at the inner and outer surfaces of the porous mixture in Configurations 1 and 2 (Figures 12), as a result of relatively close overall strains (e_{rr}, $e_{\varphi\varphi}$) at r and r_i. The shear displacements are in the range Δ ~ 100-600 μm and the shearband thicknesses δ vary between 5 and 10 μm for Configuration 1, 10-20 μm for Configuration 2 . This enables the evaluation of shear strains according to Eqn. 6. The shear strains are found to be in the range 10-100 (Nesterenko, Meyers et al., 1994, 1995).

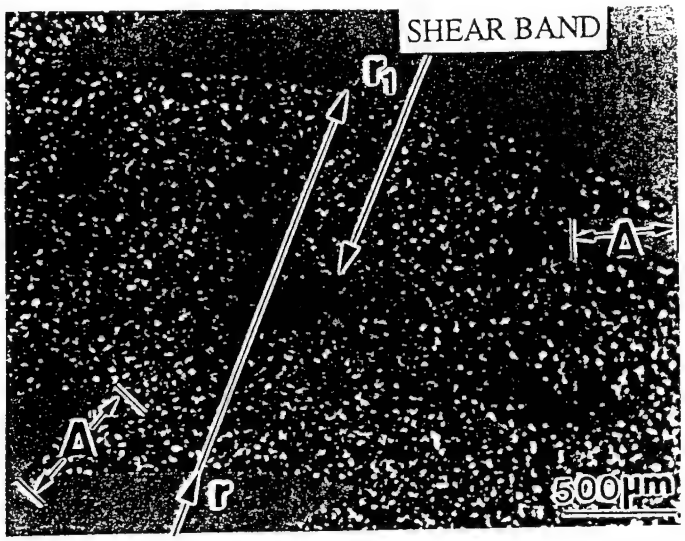

FIGURE 12. Close-up of shear localization region with displacements Δ and Δ'.

The average shear strain rate inside the shear zone can be determined from the measurement of the time of the deformation process (time of pore collapse t ≈ 8 ms) and shear strain g :

$$\dot{\gamma} \approx \frac{\gamma}{\tau} \qquad (6)$$

Shear strain rates are 10^6 - 10^7 sec^{-1} for shear bands with different values of Δ and δ.

Controlled pressure-shear experiments will be carried out for reactive porous mixtures using the thick - walled cylinder method modified for powder gun conditions. It will allow to measure the stress history of deformed material and incorporation of diagnostic by thermocouple and optical methods to monotor the reactions. Plans are under way to transition a powder gun from NAWCWPNS, China Lake for shock chemistry experiments.

IV. ACCOMPLISHMENTS DURING THIS CONTRACT

4.1 Nb - Si Mixture

This mixture represents the reactant materials with relatively small heat of reaction (enthalpy of reaction 138 kJ / mol) and was thoroughly investigated under shock-wave conditions (Meyers, Vecchio, and Yu, 1994). Using the thick - walled cylinder it was demonstrated that densified Nb-Si mixtures deform plastically, at high strain rates, by shear

localization (Configuration 1, Figure 7a,b). Furthermore, it was possible to promote localized shear in a Nb- Si mixture (initially less dense than in Configuration 1) by using a layer of metallic glass around the porous mixture(Configuration 2, Figure 7c) (Nesterenko et al, 1994, 1995).

The shear localization seems to induce the partial melting of one component (Si), as in shock-wave loading (Meyers, Vecchio, and Yu, 1994). This is clear from the observations of typical cracks resulting from shrinkage during solidification at the boundaries of the shear bands and from the characteristic flow of molten Si (Nesterenko, Meyers et al., 1995). The small thickness of the shear band is responsible for quenching the material from the state resulting from localized plastic deformation and chemical reactions.

The multiple fracturing of the Nb particles is due to shear localization (at the mesolevel. Subsequent self organization of shear bands (Nesterenko, Meyers, Wright, 1995) produces a unique fracture patterning inside the shear zone (Figure 13) and leads to a decrease of the initial particle size from 44 μm to 0.1 - 2 μm. The small final particle size, corresponding to shear band spacing at mesolevel, can be explained by high strain rate inside shear band (10^6 - 10^7 sec^{-1}). Strain rate determines the shear band spacing ((Nesterenko, Meyers, Wright, 1995). Shear localization inside the Nb particles results not only in fracturing, but also in intense heating of the newly created thin particles. This is

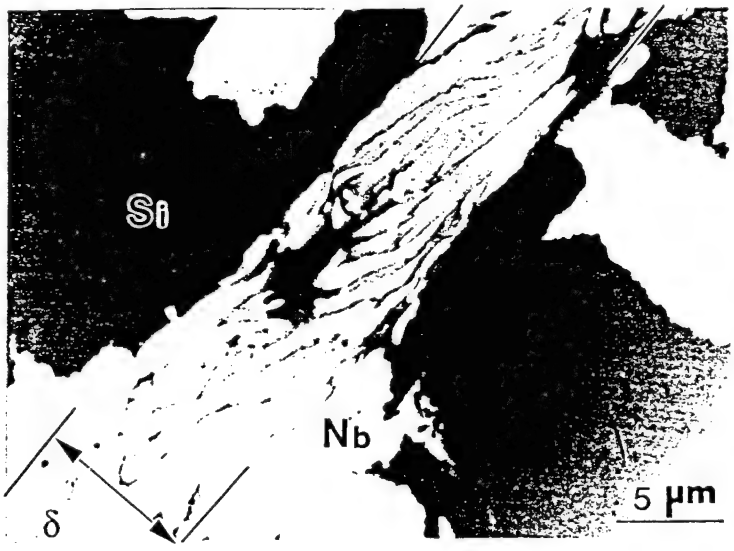

FIGURE 13. Fracture patterning of Nb particles inside shear bands (Configuration 1). Nb is white, Si is dark, and the boundaries of shear band are shown by lines on the back.

qualitatively different from the behavior of Nb particles in the mixture with Si in shock-wave compression with amplitudes up to 30 GPa and is very important for triggering of chemical reactions.

Material flow inside the shear band is unstable and results in vortex formation. Evidence for vorticity, in the form of circular patterns by the split niobium particles, was found in Configuration 1(Figure 14a) and Configuration 2(Figure 14b). Arrows in Fig.14 show the regions where the thin layers, resulting from the shear fracture of the Nb particles (white), mark the rotations in the flow pattern. Vorticity can drastically enhance the heat and mass transfer. The minimum rotational frequency w inside the vortex can be evaluated because the time for the process ($\tau \approx 8 \cdot 10^{-6}$ s) is known, as is the number of circles. From these parameters for one example (Figure 14a, vortex diameter $\approx \delta / 4 \approx 3\mu$m), the corresponding rotational frequency is $w \sim 7 \cdot 10^5$ s^{-1}. Patterning inside of the shear zone due to either thermal or non-local effects (described by high order gradient models) was recently predicted (Molinari and Leroy, 1991). It is possible that vortex formation can be explained by a non-local mechanism: gradients in flow stresses due to the heterogeneity of the mixture are a possible cause (Leroy and Molinari, 1993). An alternative explanation is based on hydrodynamic instability of the flow inside the shear zone. The upper limit of Reynolds number, Re, for material flow inside the shear band can be evaluated assuming that the Si is completely molten. The overall average velocity V of flow can be calculated as

$$V \approx \Delta / \tau \qquad (8)$$

For $\Delta \approx 600$ mm, $t \approx 8$ μs, V is approximately equal to 75 m/s. The corresponding Reynolds number for the flow inside shear band is

$$\mathrm{Re} \approx V \delta / \nu. \qquad (9)$$

Taking viscosity value for pure liquid Si in the vicinity of melting point $\nu \approx 0.4 \cdot 10^{-2}$ cm^2/s (Metals Reference Book, 1976) and $\delta \approx 10$ μm, one obtains $\mathrm{Re} \approx 1{,}900$. The hydrodynamic flow instability inside the shear band demands a critical Reynolds number between 3,100 and 4,000 (Dryden et al., 1956). This can hardly be developed under these conditions, considering that the assumed viscosity of Si is the lower limit. In some cases, the vorticity was observed in regions with partial melting of Si and without the essential reaction between Nb and Si (Figure 14b). A viscosity of the partially molten amorphous Si at around 1000 C was estimated to be 4 (10^3 - 10^4) cm^2/sec (Masaki et al., 1994), giving Reynolds numbers 6 to 7 orders of magnitude less than necessary for the beginning of turbulent flow in

the geometry of observed shear bands. Nevertheless, this mechanism cannot be ignored because material inside the shear band is not homogeneous and therefore the shear thickness is not uniform.

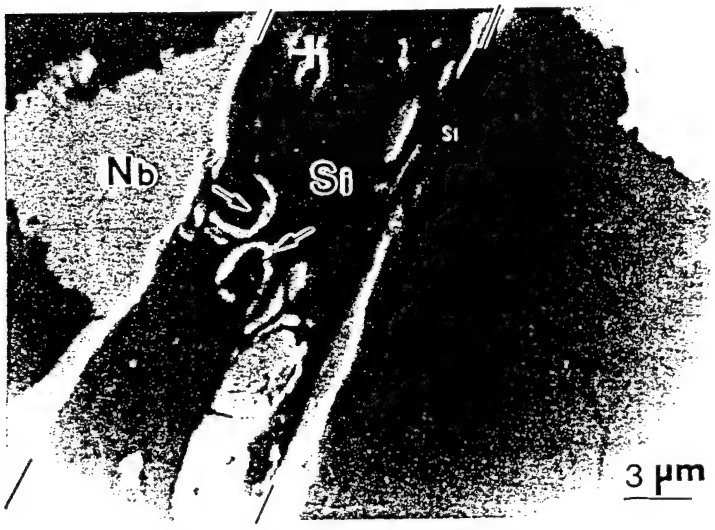

a

b

FIGURE 14. Vorticity formation (arrows) inside the shear band for (a) Configuration 1 and (b) for Configuration 2.

The intermetallic reaction between molten Si and fractured Nb proceeded in some regions (Figure 15a-d): the interior of cracks in Nb and small rounded particles inside Si with diameters less than 8 mm are favored sites. These reaction spots were identified by energy dispersive X-ray analysis. The analysis indicates that the reaction products shown in Figures 15a,b and c are Nb-rich phases (composition falls into the two-phase field of Nb_5Si_3 + $NbSi_2$) and Figure 15d is Si-rich phase (composition corresponds to two-phase field $NbSi_2$ +Si). All of the reacted products have a rounded shape. In some cases, a central cavity can be seen, which provides experimental support for a liquid state of the reaction products just after reaction because the void would be caused by solidification shrinkage. A qualitative difference between shear-band structure for Configurations 1 and 2 (having different initial densities) was observed. Reaction products with sizes up to 8 μm (Figure 15 a,b,d) were observed only for Configuration 2. This can be explained by relatively larger shear band thicknesses resulting in more intense turbulent motions and an increase in the cooling time, as well as more intense heating during the uniform stage of deformation and essential densification. A higher initial powder density, resulting in smaller shear thickness, provides a faster cooling rate that inhibits the reaction in Configuration 1. Another interesting phenomenon which should be mentioned is that, in Configuration 2, reaction products have approximately the same maximum sizes independent on the displacement Δ (Figures 15 a,b correspond to "large" shear band-LSB1, Figures 15 c,d to "small"-SSB5).

Reaction products can have either a microdendritic (Fig.15a, 16) or a microcrystalline structure(Fig. 15b,c,d). The difference can be explained by local variations of element content and cooling rate. Very often the reaction products were partially fragmented (Figure 15a, d), indicating that some deformation continued after the reaction was extinguished. At the same time, the absence of intense shear displacements (which were able to cut Nb particles, Figure 13) clearly demonstrates that reaction products were formed after the main stage of shear deformation. In an analogy to the classification of chemical reactions resulting from shock loading by Thadhani (1994), the observed reactions can be called *shear-assisted* chemical reactions.

Reactions were not observed outside the shear zones for any of the configurations for investigated regimes of plastic deformation of Nb - Si mixture. These results are in accord with a recent report of shock-induced formation of $MgAl_2O_4$ spinel upon shock loading of single crystals(corundum-Al_2O_3 and periclase-MgO) by Potter and Ahrens 1994. In oblique impact experiments, up to a velocity providing a pressure in the 26-36 GPa range, reaction products were observed at the impact interface. It is probable that shear deformation also played an important role in these experiments.

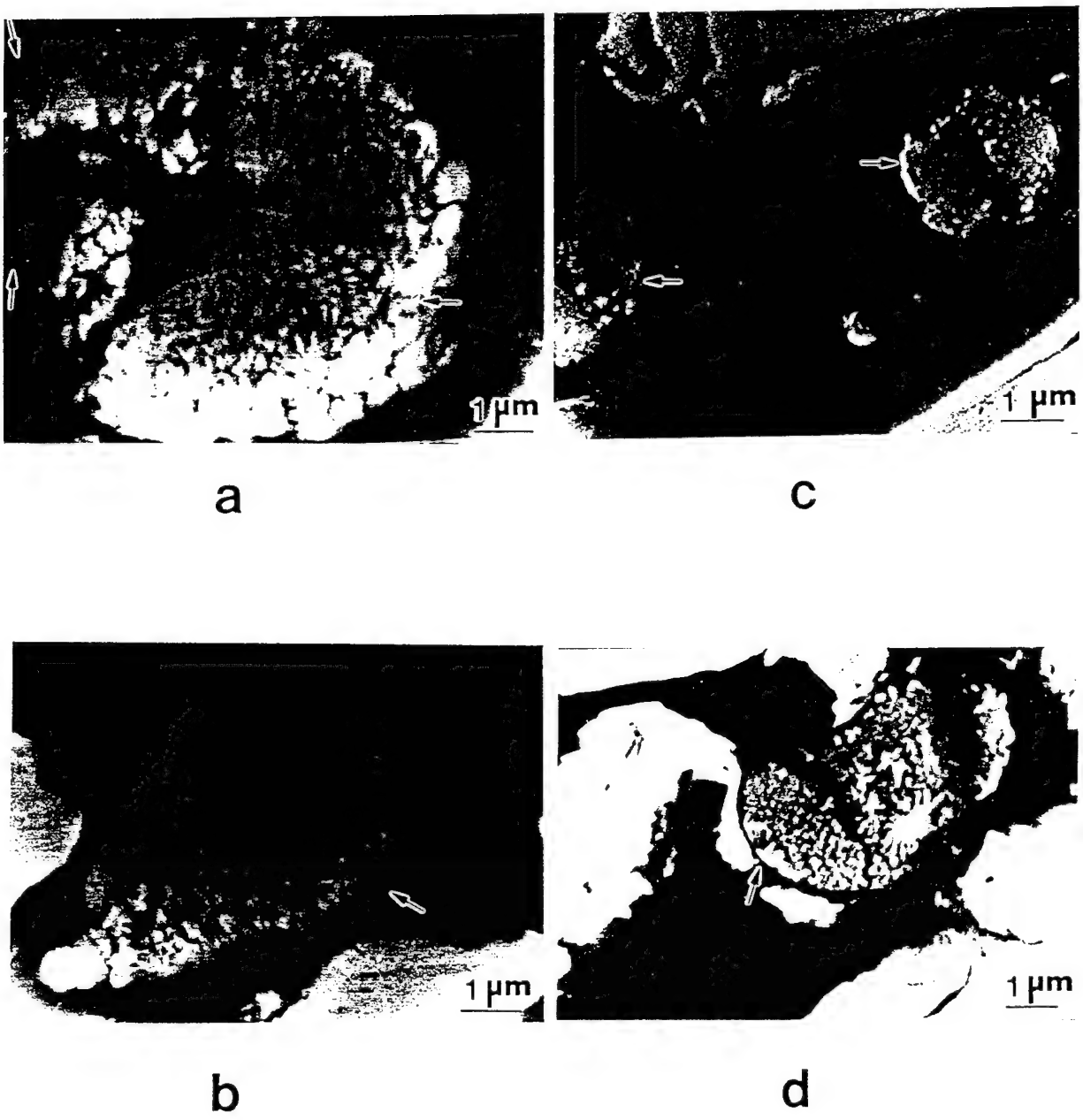

FIGURE 15. Partially reacted material (arrows) inside the shear band, Configuration 2; (a), (b) and (c) Nb-rich phase and (d) Si-rich phase in the Nb - Si system.

FIGURE 16. Dendrite structure with secondary dendrite arm spacings $\lambda \sim 0.1$ μm; the reacted particle is the same one as in Fig. 15a.

4.2 Ti -Si Mixture

The enthalpy of reaction for the Ti - Si system is four times larger (580 kJ / mol) than for Nb - Si, suggesting that under the same deformation conditions reaction would be much more generalized. Experimental results for Ti - Si system are presented in Table 1.

Experiments were carried out at increasing strains. They can be prescribed by varying the diameter of the central orifice in Stage 2 of Configuration 1 or by placing an internal cylinder inside orifice as in Configuration 3 (Figure 7d). Global true strains were varied between 0.19 and 0.35. It is important to note that the local strains in the localized shear regions are much higher and can exceed 10. No shear localization was found for a global strain $\varepsilon_{eff} \sim 0.24$.

Table 1

Thick-walled cylinder (Configuration 1) experiments carried out for Ti-Si mixture.

Global strain (in Stage 2)	*Reaction*
0.19	No
0.24	No
0.31	Only inside shear bands
0.33	Full
0.35	Full

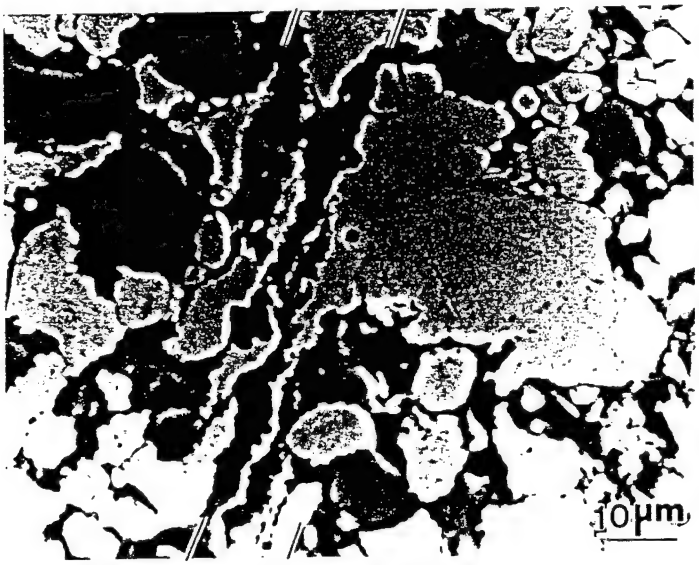

FIGURE 17. Mesolevel incipient shear inside the plastically deformed layer, global strain on inner surface of the sample $\varepsilon_{eff} \sim 0.24$. No well developed shear bands.

Under these conditions, only an incipient shear was observed inside porous layer, probably as a result of material nonuniformity or fracture of Si particles (Figure 17).

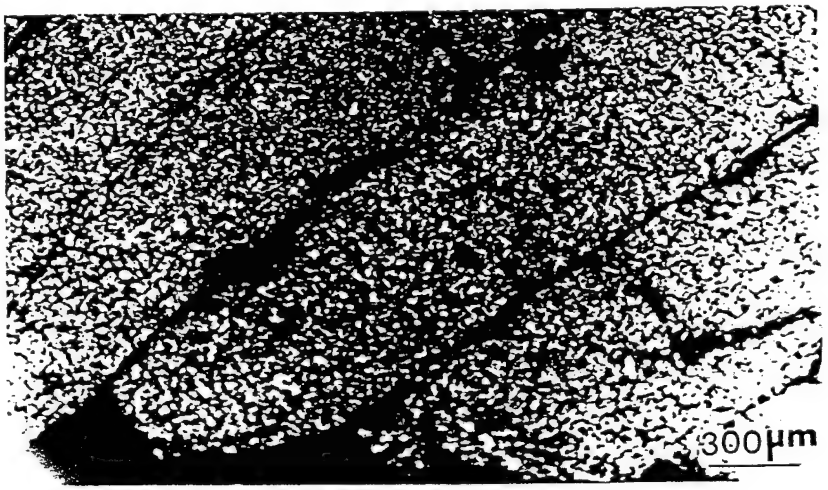

FIGURE 18. Array of shear bands below the global deformation threshold for overall chemical reaction, and above threshold for uniform deformation, $\varepsilon_{eff} \sim 0.31$.

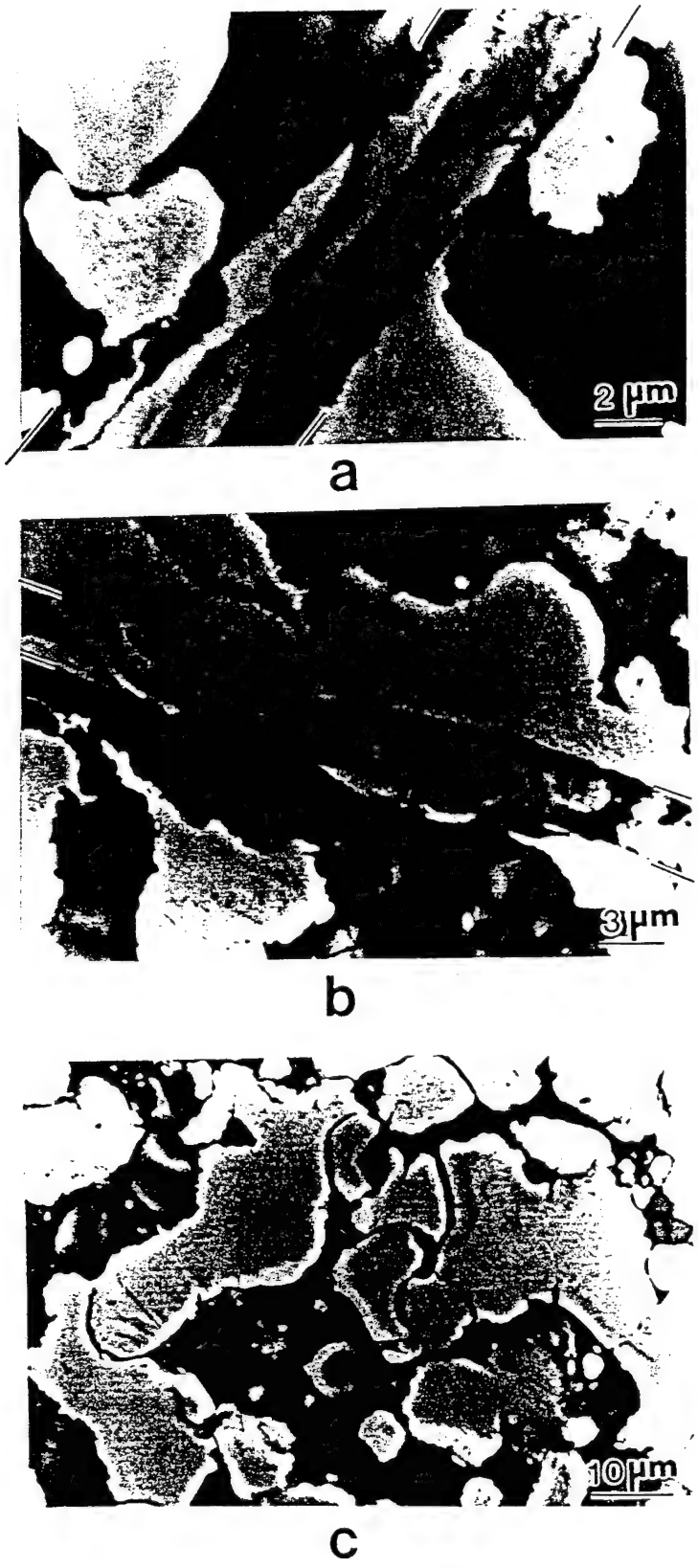

FIGURE 19. (a) and (b) - Partial reaction inside shear bands; - (c) - no reaction outside shear bands; $\varepsilon_{eff} \sim 0.31$.

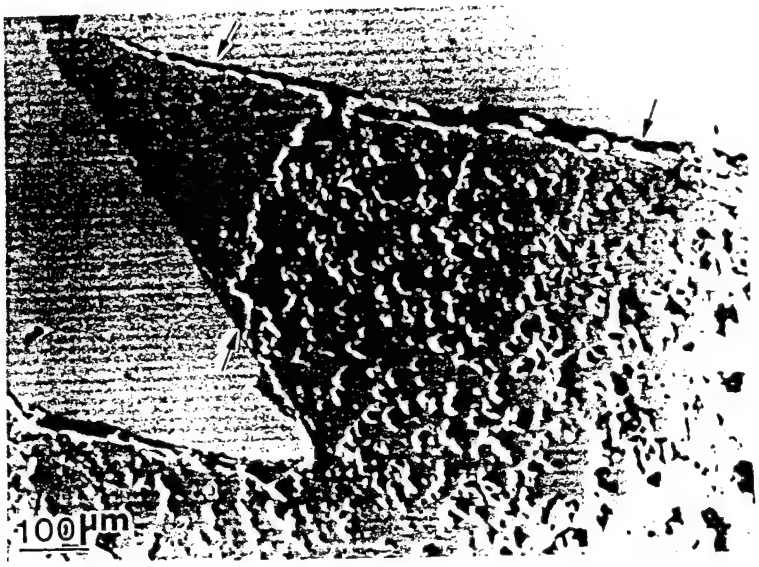

a

b

FIGURE 20. Completely reacted material in Ti - Si mixture. Small unreacted islands are shown by arrrows, $\varepsilon_{eff} = 0.33$.

Shear localization starts at global strains between 0.24 and 0.31 (Figure 18). For a plastic strain of 0.31, partially reacted material was found only inside shear bands (Figure

19a,b). Outside shear band no reaction was observed (Figure 19c). This behavior is similar to the behavior of Nb - Si at larger deformation (Figure 15). The deformation features of Ti particles (multiple fracturing and extensive plastic flow) are also similar. Unlike in the Nb-Si mixture, the reaction propagated throughout most of the specimen if global effective deformation was 0.31. Small triangular regions, adjacent to the copper wall (shown by arrows in Figure 20a) remained unreacted, due to rapid heat extraction by the copper wall. The structure of reacted compact near the interface with unreacted material at larger magnification is depicted in Figure 20b.

It can be seen that the strain threshold for complete reaction in the Ti - Si mixture (0.33) is very close to the threshold for localized shear deformation (0.31). Our method enables very precise tuning of the global strains and to work inside the threshold transition.

The average values of Vickers microhardness, measured in mixtures after different stages are: 177 (Configuration 1, stage 1), 914 (Configuration 1, after collapse), and 970 (Configuration 2). This significant increase demonstrates that reaction took place for Configuration 1(after collapse) and Configuration 2, where shear localization was assisted by layer of amorphous material. Shock amplitude was kept below the threshold for shock induced initiation of chemical reaction. In the absence of significant plastic flow by shear localization no reaction was observed under the same loading conditions.

4.3 Mechanism of Chemical Reaction Inside Shear Band

On the basis of the observations, a mechanism of *shear-assisted* chemical reaction leading to the product size with an order of magnitude close to the shear band thickness d can be proposed; the main stages are as follows:

(1) Niobium (Titanium) particles are split into foils with thickness on the order of magnitude of (0.1-1) mm by localized mesoshears; small Nb (Ti) particles with approximately the same sizes are also created as a result of this process. These foils and particles are heated as a result of intense shear deformation which precedes their formation during plastic fracture and have "fresh" surfaces, not contaminated by oxides.

(2) Silicon particles are molten and reaction begins due to the extensive relative flow of Nb particles and molten Si inside the shear band, in a similar manner to the mechanism proposed for shock-induced reactions (Dremin and Breusov, 1968). The reaction proceeds along the Nb (Ti) (sliver) - Si interface, with thickness l_r up to 1μm size; thus, the Nb (Ti) sliver is at least partially transformed into the reaction product. The ROLLER model proposed

by Dremin and Breusov (1968) can be a possible mechanochemical mechanism of reaction on this scale.

(3) Instability of gradient flow on a larger scale inside the shear band results in vorticity and coiling of partially reacted Nb foils (as snow balls) together with adjacent Si into rounded particles with diameters up to 8 μm. Vorticity can also promote the collection of partially reacted small particles to the center of rotation, providing a typical size of reaction product on the order of 1 μm. For Ti - Si mixture as result of the relatively thin shear bands, no vorticity was observed.

(4) Reaction continues up to the length D_r in places where temperatures are sufficiently high and is then quenched by thermal diffusion into the relatively cold surrounding material.

This mechanism enables the evaluation of the diameter of final reaction product, D_r, taking into account that it is equal to l_r , then multiplied by the number of rotations in the vortex:

$$D_r \approx l_r \, \omega \, \tau \, . \tag{10}$$

The relations between V, δ , w and D are:

$$\omega \approx \frac{V}{\delta}, \; \tau \approx \frac{\Delta}{V}, \; \gamma \approx \frac{\Delta}{\delta} \; . \tag{11}$$

Using Equations 10 and 11 an expression for the largest size of reaction product can be obtained in terms of the shear strain g and reaction size l_r on the lower scale:

$$D_r \approx l_r \gamma . \tag{12}$$

Equation 12 clearly demonstrates that the size of the reaction product is proportional to the shear. For the current experiments, γ can be equal to 100 and this can provide the essential difference in scale between l_r and D_r. It is important to emphasize that Equation 12 represents the connection between the size of the reaction region at the microlevel and the dimensions of the reacted particles at the macrolevel determined by the mechanical shear movement of material.

An analogous relation for the sizes of reaction products can be applied between any adjacent structural levels (for example, between scale l_r and some lower level) if the corresponding shear deformation exists on an upper scale. The main attributes of the mechanism are in qualitative agreement with the proposed phenomenological CONMAH (Graham, 1993) model for shock-wave loading.

4.4 Evaluation of Time Window for Chemical Reactions

4.4.1 Reaction time inside shear bands

Heat conductivity evaluation. The time of reaction inside shear bands can be evaluated from the time of quenching of hot material inside it. For the Nb-Si system reaction was quenched as a result of heat removal to the relatively cold material outside the shear band. Taking the thermal diffusivity for surrounding material as $k \sim 0.1\ cm^2/s$, $\delta \approx 10\ \mu m$ (Figures 12 - 14, 18), the quenching time and rate t_q and $\dot{T}$ are obtained:

$$t_q \sim \delta^2 / k \sim 10^{-5}\ s \qquad (13)$$

$$\dot{T} \sim \Delta T/t_q \sim 10^3\ K / 10^{-5}\ s \sim 10^8\ K/s \qquad (14)$$

Secondary dendride arm spacing evaluation. The dendritic structure of the reaction product with evident secondary dendrite arm spacings λ (Figure 16) enables the evaluation of cooling rate $\dot{T}$ (K/s). Since the dendrite-coarsening during the stage of cooling can be neglected, λ can be used for calibrating very fast cooling rates by extrapolation from slower, well-determined cooling rates, using the relation (Cahn, 1983):

$$\lambda \dot{T}^{1/3} = const. \qquad (15)$$

The value of constant in Eqn. 15 for Nb-Si system is unknown, but for a qualitative evaluation, one can use the available data (Cahn, 1983) for Al-7 to 11 wt% Si, equal 50 $\mu m(K / s)^{1/3}$. Using this value and $\lambda \approx 0.1\ \mu m$ (Figure 9) one obtains $\dot{T} \approx 10^8\ K / s$, which is in good agreement with the cooling rate calculated from the ratio of the temperature drop during cooling ($\sim 10^3$ K) and the previously estimated cooling time(based on the small shear band thickness), which is close to the deformation process time (10^{-5} s). These estimates confirm that despite the fact that reaction products(as can be concluded from their shape after deformation) and the dendrites were formed after the main stage of the shear deformation, they nevertheless were formed in the same time scale of 10^{-5} s. In Ti - Si mixture we did not observe secondary dendrites in reaction products.

It is worthwhile to mention that only the beginning of spherule formation is noticeable in Figures. 15a and 16, being very well developed for shock assisted chemical reactions for the same materials (Meyers, Vecchio and Yu, 1994).

4.4.2 Reaction time for entire material

The material instability resulting in shear band development creates a new space scale L (spacing between shear bands) which is able drastically reduce the time of bulk reaction. This is why the characteristic time of the reaction for whole sample t_s can be evaluated as

$$t_s = L / 2C \qquad (16)$$

where C is the propagation rate for SHS reactions and 1/2 is due to the fact that reaction propagates from two adjacent shear bands.

In our case reaction propagated in relatively dense material; the density is approximately 80 to 90 percent after initial precompaction in Stage 1. The existing experimental data for different mixtures involving Ti (Rice, Richardson, Kunetz, Schroeter, and McDonough 1986) indicate that propagation rate for SHS reactions reaches a maximum at 50 - 70 % theoretical density of the reactant compact and then decreases to zero under further increase of density to 90 %. Lack of ignition, slow propagation or even reaction decay were observed by these investigators in experiments with cold rolled powders. Even if the reaction started in a material at 50 to 70 % of theoretical density it extinguished itself in adjacent section of material with 90 % theoretical density.

These preliminary results indicate that material has enhanced reactivity after high-strain-rate plastic deformation. The reaction ceased only in layers adjacent to copper tube (Figure 20). The maximum reported rate for reaction $Ti + 2B \rightarrow TiB_2$ is equal 8 cm/s at 70 % theoretical density (Rice, et al., 1986). The spacings between shear bands in our expriments, L, were approximately equal to 0.05 cm (Figure 17). Taking C = 8 cm/s and L = 0.05 cm/s, the the reaction time t_s for entire sample using Eqn. 16 is equal to 3 ms.

Smaller reaction times should be expected because the rate of reaction exceeds 8 cm/s in plastically deformed material. The propagation rate for SHS systems can be equal 200 cm / s in thin multilayer material (Dyer, Munir, and Ruth, 1994). It is also possible to decrease the shear band spacings L by increasing the strain rate (Nesterenko, Wright, and Meyers, 1995). The initiation of reaction by shear bands can be combined with subsequent shock loading of mixture or shock loading can precede the rapid plastic flow.

It is possible to evaluate the expected time of energy release under conditions allowing the spacing between shear bands in the range 200 - 500 μm : 100 microseconds. Thus, it may be concluded that tailoring of the reaction time is feasible under dynamic plastic deformation.

4.5 Publications and Other Results

The following papers have been prepared, accepted and published:

1. V.F. Nesterenko, M.A. Meyers, H.C. Chen, and J.C. LaSalvia, "Controlled High-Rate Localized Shear in Porous Reactive Media", *Applied Physics Letters,* December 12, 1994, vol. 65, (no. 24), p. 3069-3071.

2. V.F. Nesterenko, M.A. Meyers, C.H. Chen, and J.LaSalvia, "The Structure of Controlled Shear Bands in Dynamically Deformed Reactive Mixtures", *Metallurgical and Materials Transactions A,* 1995, vol. 26A, October, p. 2511-2519 .

3. H.C. Chen, M.A. Meyers, and V.F. Nesterenko, "Chemical Reaction in Ti-Si Mixture under Controlled High-Strain-Rate Plastic Deformation", *Proceedings of International Conference EXPLOMET-95,* El Paso, August 6-10, 1995, Elsevier Science B.V., pp. 723-730.

4. V.F. Nesterenko, M.A. Meyers, Y.J. Chen, and J.C. LaSalvia, "Chemical Reactions in Controlled High-Strain-Rate Shear Bands", *Proceedings of American Physical Society Topical Group on Shock Compression of Condensed Matter Conference,* Seattle, August 13-18, 1995(in press).

5. V.F. Nesterenko, M.A. Meyers, and T.W. Wright, "Self-Organization of Shear Bands in High-Strain-Rate Deformation"(submitted to *Acta metall. mater.)* (in English).

6. V.F. Nesterenko, M.A. Meyers, and H.C. Chen, "Shear Localization in High-Strain-Rate Deformation of Granular Alumina", *Acta metall. mater.* (in press) .

7. V.F. Nesterenko, "Dynamic Loading of Porous Materials: Potential and Restrictions for Novel Materials Applications", *Proceedings of International Conference EXPLOMET-95,* El Paso, August 6-10, 1995, Elsevier Science B.V., pp. 3-13.

8. V.F. Nesterenko, M. A. Meyers, and T.W. Wright, "Collective Behavior of Shear Bands", *Proceedings of International Conference EXPLOMET-95,* El Paso, August 6-10, 1995, Elsevier Science B. V., pp. 397-404.

9. D.J. Benson, V.F. Nesterenko, and F. Jonsdottir, "Numerical Simulations of Dynamic Compaction", *Proceedings of the Net Shape Processing of Powder Materials Symposium, ASME International Mechanical Engineering Congress and Exposition*, San Francisco, Nov. 12-17, 1995.

10. H.C. Chen, M.A. Meyers, and V.F. Nesterenko, "Shear Localization in Granular and Comminuted Alumina", *Proceedings of American Physical Society Topical Group on Shock Compression of Condensed Matter Conference*, Seattle, Aug., 13-18, 1995(in press).

The book "Dynamics of Heterogeneous Materials" is 60pct completed (see APPENDIX) and is expected to be finished to the end of this year.

The novel experimental configuration called Thick-Walled Cylinder method was succesfully applied for materials testing, including monocrystals, Ti, Ta, reactant mixtures and comminuted materials. The future development of this technique for gas gun conditions is very feasible.

The course "Dynamic Behavior of Materials" was succesfully taught in the Spring of 1995.

V.CONCLUSIONS

The thick-walled cylinder method was successfully applied to generate controlled, high-rate localized reactive shear bands in heterogeneous, porous materials with overall parameters inside shear bands up to $\gamma = 100$, $\dot{\gamma} = 10^7$ sec^{-1}. A new mechanism of *shear-assisted* chemical reaction, qualitatively different from the one observed for shock-wave loading, is proposed. It predicts a linear dependence of the reaction product size on shear strain. For Nb-Si mixtures reaction was restricted to shear bands, but for Ti-Si system(with a heat of reaction three times higher) the reaction, initiated inside shear bands propagated throughout the entire specimens (with the exception of small regions, adjacent to copper driver tube, where it was arrested due to rapid heat transfer).

The visit of Prof. V. Nesterenko, with a duration of 24 months, was concluded with success. He is now on the faculty of the Department of Applied Mechanics and Engineering Sciences as Associate Professor in Residence. The project will hopefully be continued under ONR funding. A proposal was submitted to Dr. J. Goldwasser.

VI. REFERENCES

Adadurov G.A., Barkalov I.M., Goldanskii V.I., Dremin A.N., Ignatovich T.N., Mikhailov A.M., Talroze V.I., and Tampolskii P.A., *Polymer Sci. USSR*, **7**, 196, 1965.

Bancroft D., Peterson E.L., and Minshall S., *J. Appl. Phys.*, **27**, 291, 1957.

Batsanov S.S., and Deribas A.A., *Combustion, Explosion and Shock Waves*, **1**, 77, 1965.

Batsanov S.S., Doronin G. S., Klochkov S. V., and Teut A. I., *Comb., Expl. and Shock Waves*, **22**, 765, 1986.

Batsanov S. S., Gogulya M.F., Braznikov M.A., Lazareva E.V., Doronin G.S., Klochkov S.V., Banshikova M.B., Fedorov A.V., and Simakov G.V., *Sov. J. Chem. Phys.*, **10**, 1699, 1991.

Batsanov S. S., *Effects of Explosions on Materials*, Springer-Verlag, New York, 1993.

Boslough M.B., *J. Chem. Phys.*, **92**, 1839, 1990.

Bowden F.P. and Yoffe A.D., *Fast Reactions in Solids*, Butterworths, London, 1958.

Bridgman P.W., *Phys. Rev.*, **48**, 825, 1935.

Bridgman P.W., *Proc. Am. Acad. Arts Sci.*, **71**, 9, 1937.

Bridgman P.W., *J. Chem.Phys.*, **15**, 311, 1947.

Bridgman P.W., *The Physics of High Pressure*, Bell, London, 1949.

Chen H.C., Meyers M.A., and Nesterenko V.F., in *Metallurgical and Materials Applications of Shock-Wave and High-Strain-Rate Phenomena*, Eds. L.E. Murr, K.P. Staudhammer, and M.A. Meyers, Elsevier Science B.V. 723, 1995.

DeCarli P. S., U.S. Patent No. 3, 238, 019, March 1, 1966.

DeCarli P. S., and J.C. Jamieson, *Science*, **133**, 1821, 1961.

Dremin A.N., and Breusov O.N., *Russ. Chem. Rev.*, **37**, 392, 1968.

Duvall G., Chairman, *Shock Compression Chemistry in Materials Synthesis and Processing*, National Materials Advisory Board, NMAB-414, WA, Natl. Acad. Press, 1984.

Dyer T.S., Munir Z.A., and Ruth V., *Scripta Metall. et Mater.*, **30**, 1281, 1994

Enikolopyan N., Mkhitaryan A., Karagezyan A., Khzardzhyan A., *Dokl. Akad. Nauk SSSR*, **292**, 887, 1987

Enikolopyan N.S., *Dokl. Akad. Nauk SSSR*, **302**, 630, 1988.

Enikolopyan N.S., *Russ. J. Phys. Chem.*, **63**, 1261, 1989.

Field J.E., Swallowe G.M., and Heavens S.N., Proc. Roy. Soc., London, **A382**, 231, 1982.

Gilman J.J., Philosophical Magazine B, **71**, 1057, 1995.

Graham R.A., Morozin B., Venturini E.L., and Carr M.J., *Annu. Rev. Mater. Sci.*, **16**, 315, 1986.

Graham R.A., *Solids under High Pressure Shock Compression: Mechanics, Physics, and Chemistry*, Springer-Verlag, New York, NY, 1993.

Horiguchi Y., *J. Am. Ceram. Soc.*, **49**, 519, 1966.

Horie Y., in *Shock Waves in Condensed Matter - 1983*, Eds. J.R. Asay et al., Elsevier, 369, 1984.

Horie Y., and Graham R.A., and Simonsen, *Mater. Lett.*, **3**, 354, 1985.

Horie Y., and Kipp M.E., *J. Appl. Phys.*, **69**, 5718, 1988.

Horie Y., and Sawaoka, *Shock Compression Chemistry of Materials*, KTK Scientific Publ., Japan, 1993.

Krueger B.R., Mutz A.M., and Vreeland T., Jr., *J. Appl. Phys.*, **70**, 5362, 1991.

Krueger B.R., Mutz A.M., and Vreeland T., Jr.,*Metall.Ttrans.*, **23A**, 55, 1991.

Krueger B.R., and Vreeland T., in *Shock Wave and High-Strain-Rate Phenomena in Materials*, Eds., M.A. Meyers, L.E. Murr, and K.P. Staudhammer, Marcel Dekker, New York, 245, 1992.

Lange M. A., Ahrens T.J., *J. Earth Plan Sci. Lett.*, **77**, 409, 1986.

Meyers M.A., *Dynamic Behavior of Materials*, J. Wiley, New York, 640, 1994a.

Meyers M.A., Yu L.H., and Vecchio K.S., *Acta Metall. Mater.*, **42**, 715, 1994b.

Nesterenko V.F., Bondar' M.P, and Ershov I.V, in *High-Pressure Science and Technology-1993*, Edited by S.C. Schmidt, J.W. Shaner, G.A. Samara, and M. Ross, APS, pt.2, p. 1173.

Nesterenko V.F. and Bondar' M.P., *Combustion, Explosion, and Shock Waves*, **30**, 500, 1994a.

Nesterenko V.F. and Bondar' M.P., *DYMAT Journal,* **1**, 245, 1994b.

Nesterenko V.F., Meyers M.A, Chen H.C., and LaSalvia J.C., *Appl. Phy. Lett.*, **65**, 3069, 1994c.

Nesterenko V.F., Meyers M.A., Chen C., and LaSalvia J. C., *Metall. and Mater. Trans.*, **26A**, 2511, 1995

Nesterenko V.F., Meyers M.A., and Wright T.W., in *Metallurgical and Materials Applications of Shock-Wave and High-Strain-Rate Phenomena*, Eds. L.E. Murr, K.P. Staudhammer, and M.A. Meyers, Elsevier Science B.V. 397, 1995

Nesterenko V.F., Meyers M.A., Chen H..C., and LaSalvia J.C., *Proc. of American Phys. Society Topical Group on Shock Compression of Condensed Matter Conference,* Seattle, APS, 1996(in press).

Nomura Y., *Kagaku Kogyu*, **16**, 123, 1963.

Nomura Y., J. *Less-Common Metals*, **11**, 378,1966

Rice R.W., Richardson G.Y., Kunetz J.M., Schroeter T, and McDonough W. *J. Ceram. Eng. Sci.* Proc., July - August, 737, 1986

Ryabinin Yu. N., *Soviet Phys. Tech. Phys.*, **1**, 2575, 1956.

Teller E., *J. Chem. Phys.*, **36**, 901, 1962.

Thadhani N.N., *Prog. Mater. Sci.*, **37**, 117, 1992.

Thadhani N.N., *J. Appl. Phys.*, **76**, 2129, 1994.

Vecchio K.S., Yu L.H., and Meyers M.A., *Acta Metall. Mater.*, **42**, 701, 1994.

Vereshchagin L.F., Zubova E.V., and Shapochkin V.A., *Pribori i Tekhn. Esperim.*, **5**, 89, 1960.

Zhorin V.A., Nefed'ev A.V., Linskii V.A., Novikov Y.N., Stukan R.A., Volpin M.E., Gol'danskii V.I., and Enikolopyan N.S., *Dokl. Akad. Nauk SSSR*, **256**, 598, 1981.

Yu L.H., and Meyers M.A., *J. Mater. Sci.*, **26**, 601, 1991.

Yu L.H., Nellis W., Meyers M.A., and Vecchio K.S., in *Shock Compression of Condensed Matter - 1993*, Eds. S.C. Schmidt, et al., Amer. Inst. Physics, 1291, 1994.

APPENDIX

DYNAMICS OF HETEROGENEOUS MATERIALS

V. F. NESTERENKO

1. OBJECTIVES AND APPROACH

The book describes the mechanical and physical phenomena in materials under dynamic deformation with emphasis on their internal structure at the micro and mesolevels. The following aspects will be addressed: mesomechanics of viscoplastic deformation of powdered materials under impulse loading, nonlinear wave propagation in granular materials, transformation of nonlinear impulses by laminated porous and fully dense structures, heterogeneous heating and reaction of materials under impulse loading, shear localization in heterogeneous materials (including the behavior of reactant materials in controlled shear bands), collective behavior of shear bands, and analysis of application of dynamic methods to advanced materials production.

The book focuses mainly on those aspects of behavior which are qualitatively sensitive to the structure of heterogeneous materials and are based on physical experiments.

The book considers the dynamic phenomena in heterogeneous media not from a traditional "shock wave physics" (based on Hugoniot conservation equations), but from the viewpoint of nonlinear science and materials science. It takes into account the wide spectra of wave intensities, for example, from particle velocity of about 1 m/sec (granular media) to about 10^3 m/sec; the amplitude of loading is not the most important parameter.

The concept of "sonic vacuum" (Chapter 1) is developed by the author and represents a novel approach to nonlinear wave dynamics with possible practical applications for tailoring of dynamic response with changing of material structure. Chapter 4 (shear localization) is based on the latest original results of author. Both these chapters are important for understanding the damping of shock waves and compression pulses and for penetration phenomena.

Chapters 2, 3, 5 and 6 are based on the latest results of Russian scientists and involves also the critical analysis of different approaches.

Most phenomena in the dynamics of heterogeneous media can be described by scale effects, because characteristic size of inner structure has paramount importance for them.

2. OUTLINE

Introduction

Chapter 1. Propagation of Nonlinear Impulses in Elastic Particulate Materials(80% complete)

1.1 Long-wave equation for one-dimensional chain of granules
1.2 "Sonic vacuum" equation for granular chain
1.3 Stationary solutions for "sonic vacuum" equation
1.4 The stability of nonlinear periodic waves in chain of granules
1.5 Computer calculations for wave dynamics of unstressed one-dimensional granular materials
1.6 Behavior of impulses in prestressed granular materials
1.7 Randomized one-dimensional granular materials
1.8 Comparison of experimental results with computer calculations and analytical solutions
1.9 2-D, 3-D computer calculations of dynamic processes in granular materials
1.10 Soliton interactions with interface of two "sonic vacuums"
1.11 Waves in two-particle chain of granules
1.12 Power-law particulate materials - more general example of "sonic vacuum"
1.13 Particulate materials with abnormal compressibility; rarefaction solitary waves
1.14 "Sonic catastrophy" for particulate materials

Chapter 2. Micromechanics of Porous Condensed Materials under Intense Dynamic Loading(50% complete)

2.1 Experiments on dynamic behavior of powders with thermoelectric method
2.2 Kinematics of pore collapse in the frame of Carroll-Holt model; comparison with experiments
2.3 Modified Carroll-Holt model
2.4 The front width of strong shocks in granular materials
2.5 Carroll-Holt paradox
2.6 Quasistatic and dynamic deformation of powders under shock loading; concept of microkinetic energy
2.7 2-D computer calculations of dynamic powder densification
2.8 The "cold" boundary layer on the powder-monolith interface
2.9 Separation of components in mixtures under dynamic loading
2.10 Behavior of oxide films on the surfaces of granules under dynamic loading
2.11 Shear instability of pore collapse in real materials; spall in powders

Chapter 3. Transformation of Impulses in Laminated and Porous Materials(60% complete)

3.1 Experiments on shock propagation in laminar materials
3.2 Computer calculations of shock wave attenuation; the mechanism of anomalous effect of cell size

3.3 Laminated material as model for heterogeneous medium (Thouvenin model), comparison with experiment
3.4 Shock waves in laminated porous materials
3.5 Damping of explosive shock effects by porous materials; criteria for damping

Chapter 4. Shear Localization in Heterogeneous Materials(60% complete)

4.1 Experimental observation of shear localization in polycrystals and powders
4.2 Analysis of theoretical continuum approach
4.3 High-gradients models of shear localizations
4.4 Dependence of critical parameteres for localized shear on initial material structure
4.5 Behavior of reactive materials under conditions of controlled shear, "snow ball" model
4.6 Self-organization of shear bands

Chapter 5. Non-equilibrium Heating of Powders under Dynamic Loading(60% complete)

5.1 Experimental results on heterogeneous heat release at shock loading of powders
5.2 Analysis of thermodynamic models for heterogeneous heating under shock-wave deformation
5.3 Skin model and processes of thermal relaxation in shocked powders
5.4 Non-equlibrium thermodynamics of porous powder mixtures

Chapter 6. Advanced Materials Treatment by Shock Waves(50% complete)

6.1 Criteria for strong compacts under dynamic loading
6.2 Preservation of amorphous state under dynamic loading
6.3 Mechanical properties of amorphous compacts
6.4 Electromagnetic properties of amorphous compacts
6.5 Low-temperature heat treatment of explosive compacts from rapidly solidified alloys
6.6 Shock wave modification of high-T_c ceramics
6.7 Qualitative change of morphology and microstructure of submicronic nanocrystalline ceramic($ZrO_2 - Y_2O_3$)
6.8 Obtaining of supercooled states with shock wave loading
6.9 Behavior of reactive materials under shock loading, shock assisted and shock induced chemical reactions

Conclusions